Fault detection and diagnosis of a blade pitch system in a floating wind turbine based on Kalman filters and artificial neural networks

Seongpil Cho[1, 2], Minjoo Choi[3], Zhen Gao[1, 2] and Torgeir Moan[1, 2]

[1] Department of Marine Technology, Norwegian University of Science and Technology (NTNU), Trondheim, Norway.
[2] Centre for Autonomous Marine Operations and Systems (AMOS), Norwegian University of Science and Technology (NTNU), Trondheim, Norway.
[3] Division of Naval Architecture and Ocean Systems Engineering, Korea Maritime and Ocean University, Busan, Republic of Korea.

Abstract

This paper describes the development of a fault detection and diagnosis method to automatically identify different fault conditions of a hydraulic blade pitch system in a spar-type floating wind turbine. For fault detection, a Kalman filter is employed to estimate the blade pitch angle and valve spool position of the blade pitch system. The fault diagnosis scheme is based on an artificial neural network method with supervised learning that is capable of diagnosing a predetermined fault type. The neural network algorithm produces a predictive model with training, validation and test procedures after the final performance evaluation. The validation and test procedures of the artificial neural network model are conducted with the training model to prove the model performance. The proposed method is demonstrated in case studies of a spar floating wind turbine with stochastic wind and wave conditions and with consideration of six different types of faults, such as biases and fixed outputs in pitch sensors and excessive friction, slit-lock, wrong voltage, and circuit shortage in actuators. The fault diagnosis results from the final performance evaluation show that the proposed methods work effectively with good performance.

Keywords

Floating wind turbine, Hydraulic pitch system, Blade pitch actuator and sensor faults, Fault detection and diagnosis, Kalman filter, Artificial neural network

Abbreviations

ANN	artificial neural network
CM	condition monitoring
FDD	fault detection and diagnosis
IEC	International Electrotechnical Commission
KF	Kalman filter
LVDT	linear variable displacement transducer
NREL	National Renewable Energy Laboratory
OC3	Offshore Code Comparison Collaboration
PSB	bias value in the pitch sensor
PSF	fixed value in the pitch sensor
ReLU	rectified linear units
SCADA	supervisory control and data acquisition
SR	Simo-Riflex
TF	time of fault occurrence
TFDT	time of fault detection

TFDG	time of fault diagnosis
VEF	excessive friction in the valve
VSL	slit-lock in the valve
VWV	wrong voltage applied in the valve
VCS	short-circuit in the valve

1. Introduction

Interest in fault detection and diagnosis (FDD) has increased due to the focus on the need for high reliability and availability for offshore wind turbine maintenance and operation. Unexpected faults might influence system interruption in the system components, actuators, and sensors. Faults and failures change the power production efficiency, operational safety, and system behavior of wind turbines, which cause huge economic losses. Because maintenance costs account for 25-30 % of the life cycle cost for offshore wind farms [1], the reliability of an offshore wind turbine is important.

In many possible faults of the wind turbine components, the blade pitch system contributes to the failure rate and downtime of a wind turbine according to references [2-4]. The relevant faults immediately change the aerodynamic load on the blade and power production. They also affect the response of the support structures and tower. Fault diagnosis of a blade pitch system at the early stage is critical for protecting the turbine from an unexpected operational condition [5]. This approach can provide equipment failure warning in time to prevent the occurrence, escalation of the accident and effectively improve the operation and maintenance qualities [6]. Additionally, it allows for fast accommodation against faults to avoid long-term damage and provide reliable technical guarantees for the development of the wind power industry. Therefore, there are particular interests of fault monitoring, diagnosis, and fault-tolerant control in the blade pitch system [7-15]. Cho et al. [7, 8] and Noshirvani et al. [9] show a model-based fault detection and isolation for the blade pitch system based on the diagnostic observers. Especially, a condition monitoring (CM) approach of pitch systems [10-12] using a supervisory control and data acquisition (SCADA) in wind turbines has been emphasized to monitor blade pitch performance.

Generally, fault detection and diagnosis methods can determine the fault type, magnitude, location and time of detection. Fault detection techniques include two types of methods: model-based and signal-based methods [6]. A model-based method uses a system's input and output signals that are based on the mathematical or knowledge models. Based on input from the control system and measured output signals from the actual system, this method generates a residual formed as the differences in the measured system output and estimated values from the model used as a fault indicator. Qiu et al. [13] suggest a model-based approach to estimate gear fatigue life for drivetrain gearbox using SCADA data. Chen et al. [14] and Wei et al. [15] proposed a fault detection and isolation schemes using a diagnostic observer for the pitch system and drivetrain faults. A signal-based method is based on analyses of features from the measured output signals, such as sensor values. Suitable features from the measurements represent the operating conditions whether it is a normal or fault condition. Hamadache and Lee [16] propose a signal-based frequency domain approach investigating the main shaft-bearing fault detection based on absolute value principal-component analysis technique. Nejad et al. [17] show a signal-based prognostic methods for fault detection in gears and bearings in wind turbine drivetrains.

In the diagnosis procedure with data acquisition and interpretation, the diagnosis system analyzes and recognizes the fault patterns. Classification methods [6] provide a convenient approach to solve the fault diagnosis problem to classify the data into different categories by a particular pattern such as the pattern

recognition, statistical classification, approximation method, density-based method, and artificial intelligence method. Among many different methods, machine learning in the area of the artificial intelligence is a statistical method that allows a computer system to automatically perform a task without any explicit instructions and build a mathematical model of training data to make predictions or decisions. In recent years, deep learning which is one of the machine learning algorithms has lately emerged in artificial intelligence to learn convoluted structures in large, real-world data sets collected by sensors continuously online in many applications: speech recognition, object classification, computer vision, natural language processing and robotics [18].

Machine learning algorithms can also be applied to learn how to diagnose faults by a set of measurement data for training on mechanical components of wind turbines. Diagnosis methods based on machine learning can detect changes in trends and include wavelet analysis, Bayesian network, support vector machine and neural networks [19]. Recently, support vector machine [20 - 22] and fuzzy clustering methods [23, 24] have been utilized to detect and isolate faults on sensor such as force sensor, accelerometer, speed sensor located on the blade root, tower top and generator in wind turbine control system. Santos et al. [20] describes a multi-sensory system validated on a test-bed that simulates with misalignment and imbalance faults. Zeng et al. [21] and Laouti et al. [22] suggests the SVM approaches with radius basis function used as kernels for detecting and identifying actuators, sensors and process faults. Badihi et al. [23] and Simani et al. [24] present the Takagi-Sugeno fuzzy model identified from input-output measurements for fault detections and isolations.

Specifically, many researchers employ theories of an artificial neural network with multi-layer perceptron (MLP) [25-28], convolution neural network (CNN) [29, 30], recurrent neural network (RNN) [31] and auto-encoder (AE) [32, 33] to develop a reliable fault diagnosis scheme for wind turbine components, such as main bearing, gearbox, generator, and rotor blade. Kusiak et al. [25, 28] investigate a prediction methodology of turbine faults using information of SCADA systems. Wang et al. [26] and Zaher et al. [27] describe a set of anomaly-detection techniques to analyze SCADA data acquired from a wind farm and automate operators' analysis task. Bach-Andersen et al. [29][30] exploit a data-driven deep-learning system for drivetrain monitoring applications using CNN processing on complex vibration signal inputs on both rotor bearing, planetary and helical stage gear box bearings. Tautz-Weinert and Watson [31] develop a RNN-based wear process detection scheme in drivetrains with information from installed sensors. Dervilis et al. [32] and Jiang et al. [33] proposes a fault detector with deep autoencoder (DAE) to capture the nonlinear correlations from data of multiple sensor variables against noise and input fluctuation.

To conduct effective fault diagnosis for the blade pitch system of wind turbines, a hybrid fault diagnosis algorithm was developed in this paper based on a Kalman filter and artificial neural. One of the main parts of the proposed algorithm is estimation of the parameters of blade pitch systems, and these parameters indicate a healthy or faulty system using the Kalman filter with system input and output variables. Then faults were classified and identified based on the estimated parameters using an artificial neural network method and input/output variables of the system in real-time. The hybrid approach has many advantages because the Kalman filter involves less computational costs in the detection and the artificial neural network has high accuracy in the diagnosis procedure.

In this paper, Section 2 shows the floating wind turbine model, baseline controller, and hydraulic blade pitch system (including the modeling of faults). Section 3 introduces fault detection and diagnosis for the blade pitch system and test results for the FDD scheme. Section 4 provides the conclusions.

2. Case study model and methodology

2.1. Floating wind turbine model and fully coupled numerical simulation method

A floating turbine consists of a rotor, nacelle, tower, supporting structure, and mooring system. The case study model is based on an NREL 5 MW wind turbine model [34] supported by a spar buoy floater (OC3-Hywind) [35] and three catenary mooring lines as shown in Figure 1. A mooring system was used at the fairlead positions to increase the yaw stiffness. The NREL 5 MW wind turbine specifications are listed in Table 1. In addition, the OC3-Hywind floater properties are provided in Table 2.

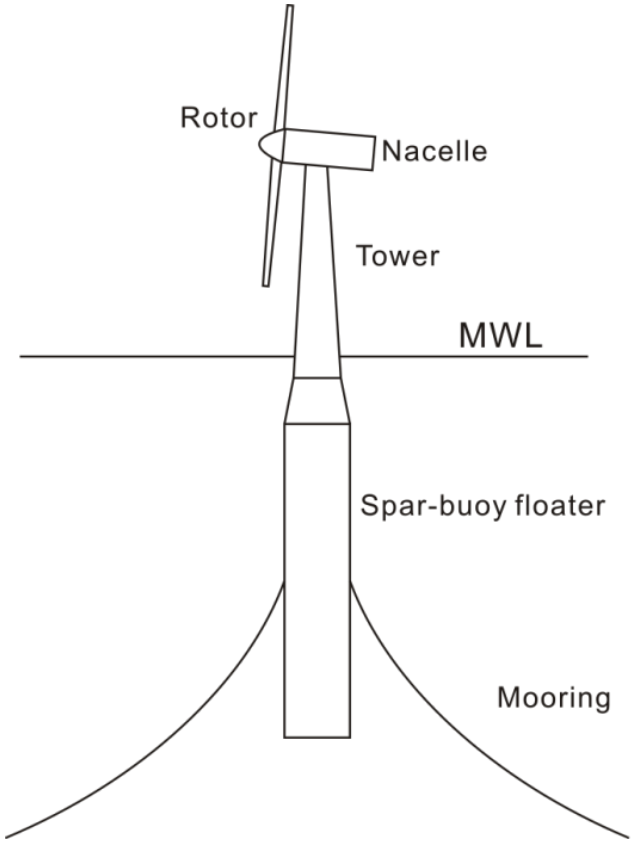

Figure 1. Schematic view of the floating wind turbine.

Table 1. Properties for the NREL 5 MW wind turbine [34].

Rated Power (MW)	5
Rotor orientation, Configuration	Upwind, 3 blades, horizontal axis
Rotor diameter (m)	126
Hub height from the mean water level (m)	90
Cut-in, rated, cut-out wind speed (m/s)	3, 11.4, 25
Cut-in, rated rotor speed (deg/s)	41.4, 72.6
Max pitch rate (deg/s)	8
Gearbox ratio	97

Table 2. Properties for the OC3-Hywind floater [35].

Water depth (m)	320
Draft (m)	120
Diameter above taper (m)	6.5
Diameter below taper (m)	9.4
Center of mass (m)	(0, 0, -89.9115)
Mass, including ballast (kg)	7.466×10^6
Mass moment of inertia, I_{xx} and I_{yy} (kg·m^2)	4.229×10^9
Mass moment of inertia, I_{zz} (kg·m^2)	1.642×10^8

The dynamic responses of the wind turbine model are conducted by using fully coupled nonlinear time-domain numerical simulations of offshore wind turbines using Simo-Riflex (SR) [36, 37], which is an aero-hydro-servo-elastic code. The hull of the spar structure is considered a rigid body with 6 degrees of freedom (heave, surge, sway, pitch, roll and yaw). Wave loads on the rigid hull, are determined based on linear potential flow theory and Morison's term for viscous (drag) as implemented in Simo [36]. Added mass, radiation damping, and first-order wave forces were obtained based on a potential flow model. Morison's drag term was used to model viscous forces. In this manner, viscous damping was included. The slender structural components, such as the blades, shaft, tower, and mooring system are modelled by beam the finite elements, accounting for geometrical nonlinear effects in Riflex [37]. The tower from the OC3-Hywind platform was modeled with 10 axisymmetric beam elements, while the blades were each modeled with 17 elements with two symmetry axes. The blade model accounted for geometric stiffening but assumed that the center of gravity, shear center, and elastic center was coincident. Moreover, the aerodynamic forces and moments on airfoil sections along the wind turbine blades based on the blade element momentum (BEM) method including tower shadow, dynamic stall, and skewed inflow correction, are accounted for [37]. Hydrodynamics, aerodynamics, structural dynamics and mooring line dynamics are considered simultaneously with a baseline control system for a pitch and torque controller and a blade pitch system under various operational conditions. Figure 2 shows the data transmission of the fully coupled model and controller [5]. Application of the fully coupled nonlinear time-domain numerical model of spar wind turbine facility is documented by references [8, 38-39] to obtain responses such as platform motions, blade-root bending moments, and tower base bending moments.

2.2 Hydraulic blade pitch actuator

The hydraulic blade pitch actuator system consists of a hydraulic pump, accumulators, directional control valves, a fluid tank and hydraulic cylinders. Each blade is equipped with an independent pitch system. The oil flow going in and out from the cylinders is controlled by a control valve. The hydraulic force in the cylinder is supplied by a hydraulic power unit placed in the nacelle.

The system controller makes a command voltage signal to control the valve spool position based on the difference between the measured blade pitch angle and the pitch angle command. A schematic diagram of a hydraulic actuator, as shown in Figure 3, consists of a pressure pump, an accumulator, a reservoir, a directional control valve and a hydraulic cylinder, as modeled in Cho et al. [5]. In this paper, a hydraulic pitch actuator is modeled and interacts with the baseline controller with modified proportional and integral gain values [35].

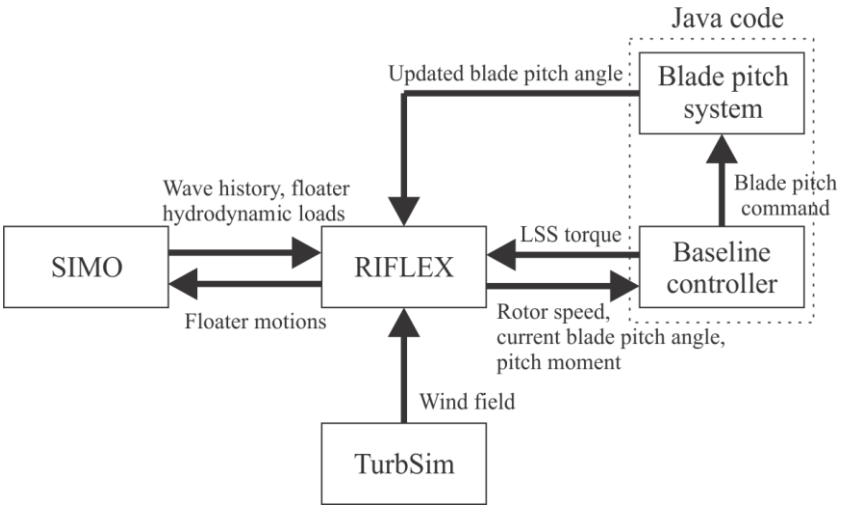

Figure 2. Data transmission between the fully coupled model and controller [5].

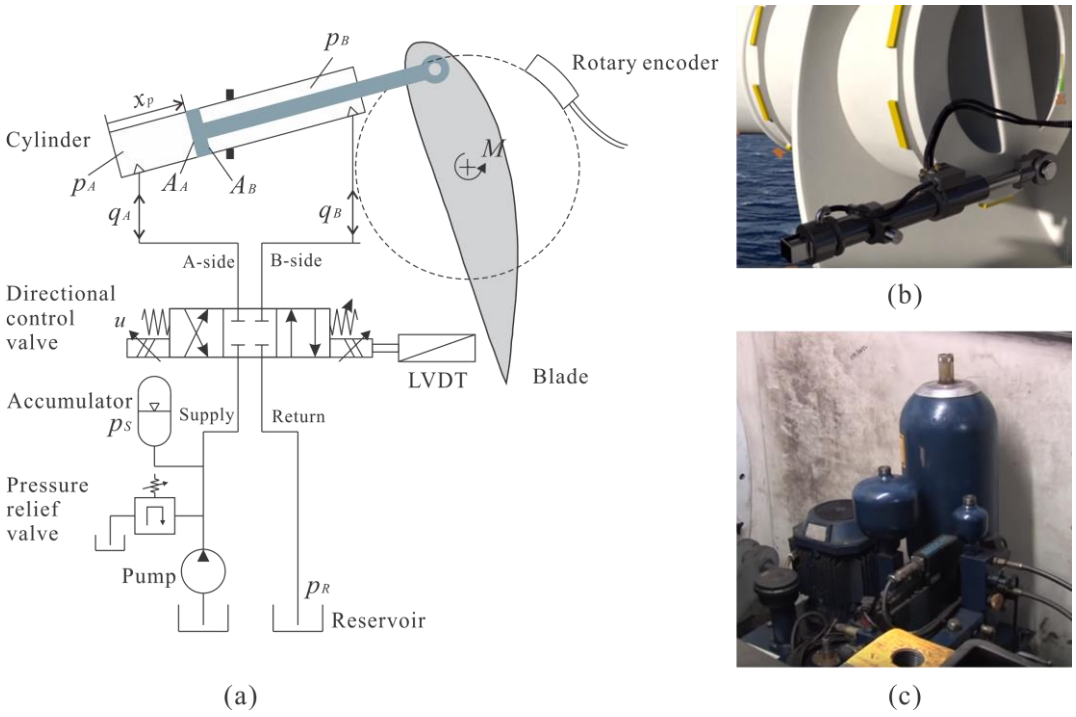

Figure 3. The hydraulic pitch system: (a) schematic diagram with sensor distributions, (b) hydraulic actuator, and (c) hydraulic power unit.

2.3. Baseline controller for operational wind turbines

The baseline control system has two controllers: the blade pitch and generator torque controllers. Below the rated wind speed, the maximum power is captured by controlling the generator torque to maintain the optimal tip speed ratio [34]. Above the rated wind speed, the blade pitch angle is controlled by the blade pitch actuator to produce a constant rated power output and to reduce aerodynamic thrust. A constant generator torque method in the baseline controller is used to improve the dynamic responses of

the system and reduce the floater motions [40]. Figure 4 shows the block diagram of the modified baseline controller, where Ω_r is the rotor speed, Ω_g is the generator speed, $\Omega_{g,m}$ is the measured generator speed, $\Omega_{g,rated}$ is the rated generator speed, Q_g is the generator torque, Q_a is the aerodynamic torque, and β_m is the measured blade pitch angle, and V_{wind} is the wind speed.

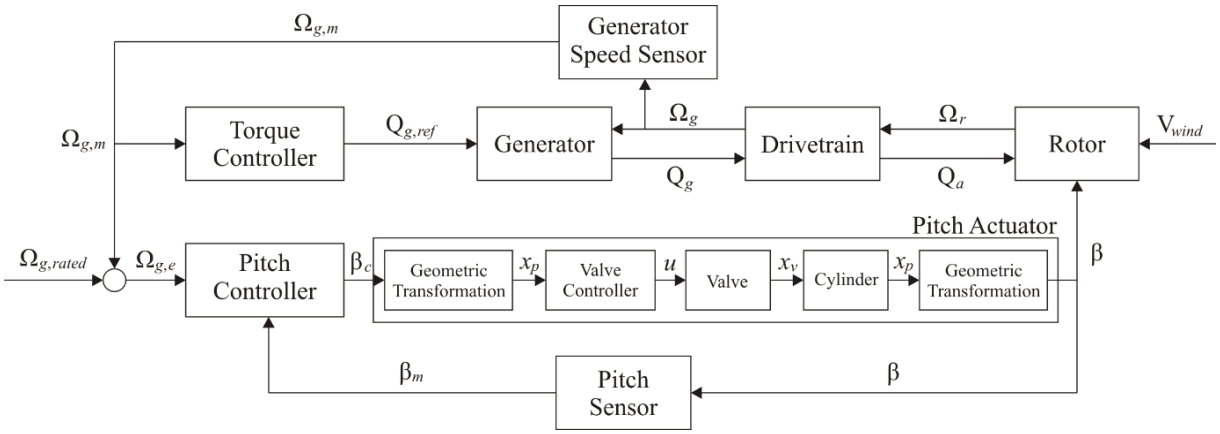

Figure 4. Block diagram of the baseline controller.

2.4. Environmental conditions

Six load cases with different wind and wave conditions were selected for simulating the dynamic responses of the floating wind turbine, as given in Table 3. In terms of the wind and wave cases, the turbulent wind field represented by the normal wind profile and the normal turbulence model is modeled by using Turbsim [41] according to the Kaimal turbulence model based on the International Electrotechnical Commission (IEC) 61400-1 [42] and 3 [43]. In the vertical plane, 32 × 32 points were used over an area of 160 × 160 m. The wind shear was modeled according to the power law with exponent 0.14. For irregular waves, the Joint North Sea Wave Project (JONSWAP) [44] wave spectrum was used. The peak period (T_p) and significant wave height (H_s) were decided based on their correlation with wind speed for the Statfjord site in the North Sea [45]. The range of the mean wind speed is in a range larger than the rated wind speed (11.2 – 24 m/s) correlated with wave conditions.

Table 3. Load cases based on winds and waves.

Load case	U_w (m/s)	Turbulence model	H_s (m)	T_p (s)
1	14	IEC Class C	3.58	10.27
2	16		3.97	10.44
3	17		4.17	10.53
4	19		4.58	10.72
5	20		4.8	10.82
6	22		5.23	11.02

3. Fault detection and diagnosis

Fault detection and diagnosis methods are described in this section. Figure 5 shows the basic structure of FDD schemes in the blade pitch system. Based on the system input command u(k) from controllers and measured data y(k) from sensors, Kalman filters estimate the states and the outputs of the blade pitch system with no fault, as shown in Eq. (5). By comparing the residual r(k) of the measured and the estimated outputs with a predefined threshold, the state and measure changes are identified. If the actual system has no fault, the residual will be close to zero. After a successful fault detection by the Kalman filter, an ANN model built from learning data diagnoses the fault type.

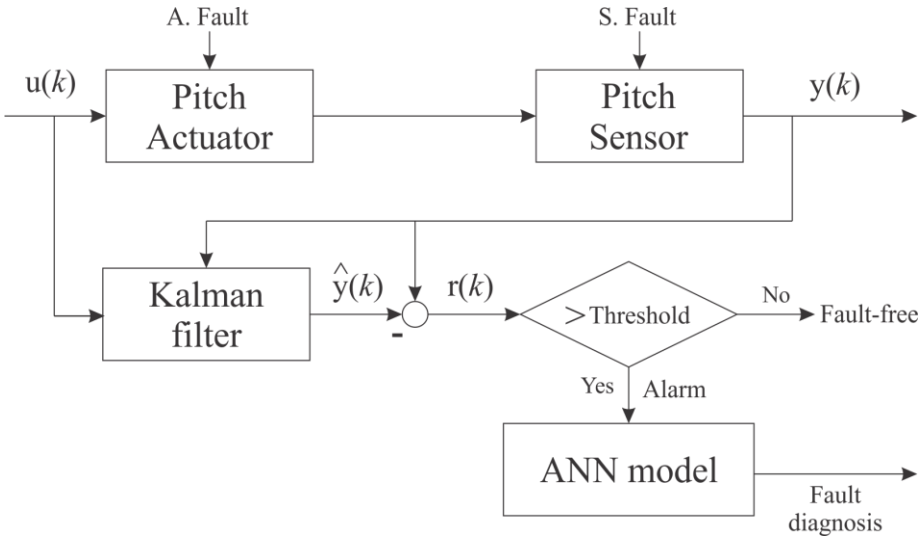

Figure 5. Overall procedure for a FDD scheme in the blade pitch systems.

3.1. Blade pitch and valve systems

The hydraulic pitch actuator with the hydraulic power unit was modeled as described in Section 2.3 from Cho et al. [5]. To estimate pitch angles and valve positions, models inserted in the Kalman filter are built as 2nd order differential equations of motion based on the equations from the hydraulic actuator [8]. The blade pitch system describes a blade pitch command from the pitch controller and the pitch angle measurement as follows:

$$\ddot{\beta}_i + 2\zeta_{bp}\omega_{bp}\dot{\beta}_i + \omega_{bp}^2\beta_i = \omega_{bp}^2\beta_{C,i}\ ,\ i = 1,\ 2 \text{ and } 3 \text{ (the blade number)}, \tag{1}$$

where ζ_{bp} is the damping ratio, ω_{bp} is the natural frequency of the pitch actuator, and ($\dot{}$) represents the time derivatives. Additionally, β_i is the i^{th} blade pitch angle, and $\beta_{C,i}$ is the blade pitch angle command. The parameters are $\zeta_{bp} = 0.6$ and $\omega_{bp} = 11.11$ rad/s [46].

The directional control valve uses an electromagnetic field via a solenoid coil to move an internal armature assembly. As the blade pitch angle command from the pitch controller varies, the control input voltage for controlling spool position eventually adjusts the hydraulic flow into the cylinder, as described in Cho et al. [5]. The valve spool position x_{vs} is calculated from the voltage u_{vs} defined by

$$\ddot{x}_{vs,i} + 2\zeta_{vs}\omega_{vs}\dot{x}_{v,i} + \omega_{vs}^2 x_{vs,i} = \omega_{vs}^2 k_u u_{vs,i}\ ,\ i = 1,\ 2 \text{ and } 3 \text{ (the blade number)}, \tag{2}$$

where ζ_{vs} is the damping ratio, ω_{vs} is the natural frequency of the valve system, and k_u is the valve gain. The parameters are $\zeta_{bp} = 0.74$, $\omega_{bp} = 141$ rad/s, and $k_u = 0.002$m/V [5, 47].

Figure 3 (a) shows a schematic diagram of the blade pitch system with the sensor distribution. To measure the blade pitch angle, incremental rotary encoders installed on the blade roots can be used. Linear variable displacement transducers (LVDTs) are used to measure the position of the valve spool. Process and measurement noises in a state-space representation of the blade pitch and valve system described by Eq. (3) are zero-mean Gaussian white noises.

$$\begin{aligned}\dot{\mathbf{x}}_{bp}(t) &= \mathbf{A}_{bp}\mathbf{x}_{bp}(t) + \mathbf{B}_{bp}\mathbf{u}_{bp}(t) + \mathbf{w}_{bp}(t)\\ \mathbf{y}_{bp}(t) &= \mathbf{C}_{bp}\mathbf{x}_{bp}(t) + \mathbf{v}_{bp}(t)\end{aligned} \tag{3a}$$

$$\begin{aligned}\dot{\mathbf{x}}_{vs}(t) &= \mathbf{A}_{vs}\mathbf{x}_{vs}(t) + \mathbf{B}_{vs}\mathbf{u}_{vs}(t) + \mathbf{w}_{vs}(t)\\ \mathbf{y}_{vs}(t) &= \mathbf{C}_{vs}\mathbf{x}_{vs}(t) + \mathbf{v}_{vs}(t)\end{aligned} \tag{3b}$$

or

$$\begin{aligned}\dot{\mathbf{x}}_{bp}(t) &= \begin{bmatrix}\dot{\boldsymbol{\beta}}_i(t)\\ \ddot{\boldsymbol{\beta}}_i(t)\end{bmatrix} = \begin{bmatrix}\mathbf{0}_{3\times3} & \mathbf{I}_{3\times3}\\ -\omega_{bp}^2\mathbf{I}_{3\times3} & -2\omega_{bp}\zeta_{bp}\mathbf{I}_{3\times3}\end{bmatrix}\begin{bmatrix}\boldsymbol{\beta}_i(t)\\ \dot{\boldsymbol{\beta}}_i(t)\end{bmatrix} + \begin{bmatrix}\mathbf{0}_{3\times3}\\ \omega_{bp}^2\mathbf{I}_{3\times3}\end{bmatrix}\boldsymbol{\beta}_{C,i}(t) + \begin{bmatrix}\mathbf{w}_{\beta,i}(t)\\ \mathbf{w}_{\dot{\beta},i}(t)\end{bmatrix}\\ \mathbf{y}_{bp}(t) &= \begin{bmatrix}\mathbf{I}_{3\times3} & \mathbf{0}_{3\times3}\end{bmatrix}\begin{bmatrix}\boldsymbol{\beta}_i(t)\\ \dot{\boldsymbol{\beta}}_i(t)\end{bmatrix} + \mathbf{v}_{bp,i}(t)\end{aligned}$$

, i = 1, 2 and 3 (3c)

$$\begin{aligned}\dot{\mathbf{x}}_{vs}(t) &= \begin{bmatrix}\dot{\mathbf{x}}_{vs,i}(t)\\ \ddot{\mathbf{x}}_{vs,i}(t)\end{bmatrix} = \begin{bmatrix}\mathbf{0}_{3\times3} & \mathbf{I}_{3\times3}\\ -\omega_{vs}^2\mathbf{I}_{3\times3} & -2\omega_{vs}\zeta_{vs}\mathbf{I}_{3\times3}\end{bmatrix}\begin{bmatrix}\mathbf{x}_{vs,i}(t)\\ \dot{\mathbf{x}}_{vs,i}(t)\end{bmatrix} + \begin{bmatrix}\mathbf{0}_{3\times3}\\ \omega_{vs}^2\mathbf{I}_{3\times3}\end{bmatrix}\mathbf{u}_{v,i}(t) + \begin{bmatrix}\mathbf{w}_{x_{vs},i}(t)\\ \mathbf{w}_{\dot{x}_{vs},i}(t)\end{bmatrix}\\ \mathbf{y}_{vs}(t) &= \begin{bmatrix}\mathbf{I}_{3\times3} & \mathbf{0}_{3\times3}\end{bmatrix}\begin{bmatrix}\mathbf{x}_{vs,i}(t)\\ \dot{\mathbf{x}}_{vs,i}(t)\end{bmatrix} + \mathbf{v}_{vs,i}(t)\end{aligned}$$

, i = 1, 2 and 3 (3d)

where the state vector is $\mathbf{x}(t)$, input vector is $\mathbf{u}(t)$ and measurement vector is $\mathbf{y}(t)$ for the blade pitch angle (*bp*) and valve position (*vs*). There are system matrices representing the state transition matrix **A**, input matrix **B** and measurement matrix **C**. Uncertain disturbances including the process noise vector $\mathbf{w}(t)$ and measurement noise vector $\mathbf{v}(t)$ are given.

3.2. Fault description

The faults in the blade pitch system can be categorized into sensor and actuator faults. Pitch sensor faults occur by dust on the encoder disc, miss-adjustment of the blade pitch bearing, operating beyond the acceptable range of temperature and humidity or improper calibration. Incorrect pitch alignment due to sensor and actuator faults leads to unbalanced rotation in the rotor causing asymmetrical forces on the blades. In the case of the pitch actuator faults, the high failure rate that is related to oil, valve and sludge issues accounts for a large portion (37.3 %) of the total failure rate for hydraulic pitch systems as shown in Carroll et. al. [3]. In addition, valve faults in the pitch actuator can change the system characteristics [48]. These faults affect the blade pitch angle and response delay. They could also affect the dynamic response of wind turbines in transient and steady-state conditions [5].

In this paper, six fault types are considered in the pitch sensor and actuator of the blade pitch system, which are described in Cho et al. [5, 8]. Table 4 describes the fault types.

Table 4. Fault description.

Fault number	Fault name	Fault occurrence location
1	Bias value (PSB)	Pitch sensor
2	Fixed output (PSF)	
3	Excessive friction (VEF)	Directional control valve
4	Slit lock on spool (VSL)	
5	Wrong voltage (VWV)	
6	Circuit shortage (VCS)	

1

2 3.3. Fault detection with a Kalman filter

3 Model-based methods detect faults by comparing the generated residual with the threshold. In this paper,
4 Kalman filters, which is often used in fault detection, satellite navigation devices, computer vision, and
5 computer games [49], are used. Using the input command $u(k)$ and measured data $y(k)$, the Kalman filter
6 estimates the states and outputs of the blade pitch system with no faults.

7 3.3.1 Kalman filter design for the system with no fault based on the discrete time-space model

8 The state-space model [8] of the blade pitch system in the discrete-time system in the pitch actuator and
9 sensor with disturbances and faults can be transferred from the proposed system (3a) and (3b), where
10 the Euler discretization approach is applied.

11
$$\begin{aligned} \mathbf{x}_j(k+1) &= \mathbf{\Phi}_j \mathbf{x}_j(k) + \mathbf{\Psi}_j \mathbf{u}_j(k) + \mathbf{\Gamma}_{f\,j} \mathbf{f}_{A\,j}(k) + \mathbf{\Gamma}_{d\,j} \mathbf{w}_j(k) \\ \mathbf{y}_j(k) &= \mathbf{H}_j \mathbf{x}_j(k) + \mathbf{\Xi}_{f\,j} \mathbf{f}_{S\,j}(k) + \mathbf{\Xi}_{d\,j} \mathbf{v}_j(k) \end{aligned}, \; j = bp,\, vs \tag{4}$$

12 where $\mathbf{\Phi}_j = \mathbf{I}_j + \mathbf{A}_j T$, $\mathbf{\Psi}_j = \mathbf{B}_j T$ and $\mathbf{H}_j = \mathbf{C}_j$ (sampling time T). Here, $\mathbf{\Phi}$, $\mathbf{\Psi}$, $\mathbf{H}$, $\mathbf{\Gamma}_d$, $\mathbf{\Gamma}_f$, $\mathbf{\Xi}_d$, and $\mathbf{\Xi}_f$ are known
13 constant matrices in a discretized system. Additionally, the actuator $\mathbf{f}_A(k)$ and sensor fault vectors $\mathbf{f}_S(k)$
14 are described in Cho et al. [8].

15 For a healthy case, the Kalman filter is designed as follows:

16
$$\begin{aligned} \hat{\mathbf{x}}_j(k+1) &= \mathbf{\Phi}_j \hat{\mathbf{x}}_j(k) + \mathbf{\Psi}_j \mathbf{u}_j(k) + \mathbf{K}_j(\mathbf{y}_j(k) - \mathbf{H}_j \hat{\mathbf{x}}_j(k)) \\ \hat{\mathbf{y}}_j(k) &= \mathbf{H}_j \hat{\mathbf{x}}_j(k) \end{aligned} \tag{5}$$

17 where $\hat{\mathbf{x}}_j(k)$ is the estimated state vector, $\hat{\mathbf{y}}_j(k)$ is the estimated output vector and $\mathbf{K}_j$ is the Kalman
18 gain matrix.

19 3.3.2 Residual generation and evaluation

20 A residual $r(k)$ is described as follows:

21
$$r(k) = y(k) - \hat{y}(k) \tag{6}$$

22 A residual energy $J(k)$ defined by the L_2 norm is described as follows:

23
$$J(k) = \left\| r(k) \right\|_{2,\Delta k} = \left(\sum_{i=k-\Delta k}^{k} r^T(\kappa) r(\kappa) dk \right)^{1/2} \tag{7}$$

The residual energy determines the fault condition by applying fault detection logic with threshold J_{th}.

$$\begin{aligned} J(k) < J_{th}, \ \text{fault} - \text{free} \\ J(k) > J_{th}, \ \text{fault} \end{aligned} \tag{8}$$

If the residual energy is less than this threshold, it indicates a fault-free state. Otherwise, it indicates a fault condition.

3.4. Fault diagnosis with the artificial neural network

3.4.1. Training, validation, and test procedures using the artificial neural network

An artificial neural network (ANN) is employed in the fault diagnosis procedure in this paper. The ANN is a framework of machine learning algorithms that automatically identify the system's characteristics from the training data. An ANN uses connected nodes called artificial neurons, which are inspired by a biological brain. In ANN implementations, artificial neurons receive input signals and process them with hidden layers that are computed by some nonlinear function for calculating the output results. Figure 6 illustrates a simple ANN. The ANN used in this paper has 100 neurons with 2 hidden layers considering time and performance of the learning procedure.

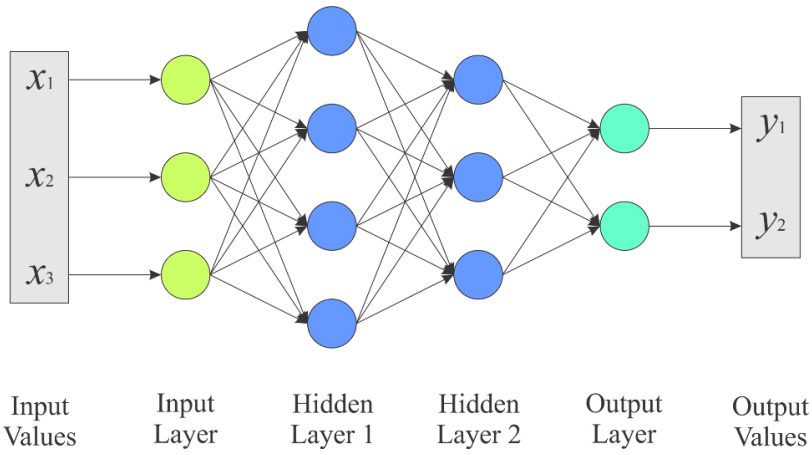

Figure 6. A simple illustration of an artificial neural network (ANN).

In this paper, an ANN determines the fault among six fault types, which are described in Table 3. In fault diagnosis using an ANN, training, validation and test procedures are essential for building the fault diagnosis model. The ANN algorithm makes the predictive model using training and validation data. Then, the final performance evaluation in terms of the accuracy of the model is conducted with test data and test label for the predictive model. Figure 7 shows the flowchart of the training, validation, and test procedures. After the learning process including training and validation procedures, the ANN library builds a predictive model that that learns certain properties from a training dataset to make those predictions. In this paper, the predictive model can be used for the fault diagnosis.

During the training procedure at each hidden layer, the rectified linear unit (ReLU) function is used as the activation function. The activation function with ReLU prevents overfitting and the gradient vanishing problem. Additionally, it reduces the computational cost. This function was found to greatly accelerate (Krizhevsky et al. [50]) the convergence of stochastic gradient descent compared to the sigmoid or tanh functions. This function returns the input value without any modification if the value is greater than 0; otherwise, it returns 0. Eq. (9) defines the function, where h_i is the i-th hidden layer value.

$$\mathrm{Relu}(h_i) = \max(0, h_i) \tag{9}$$

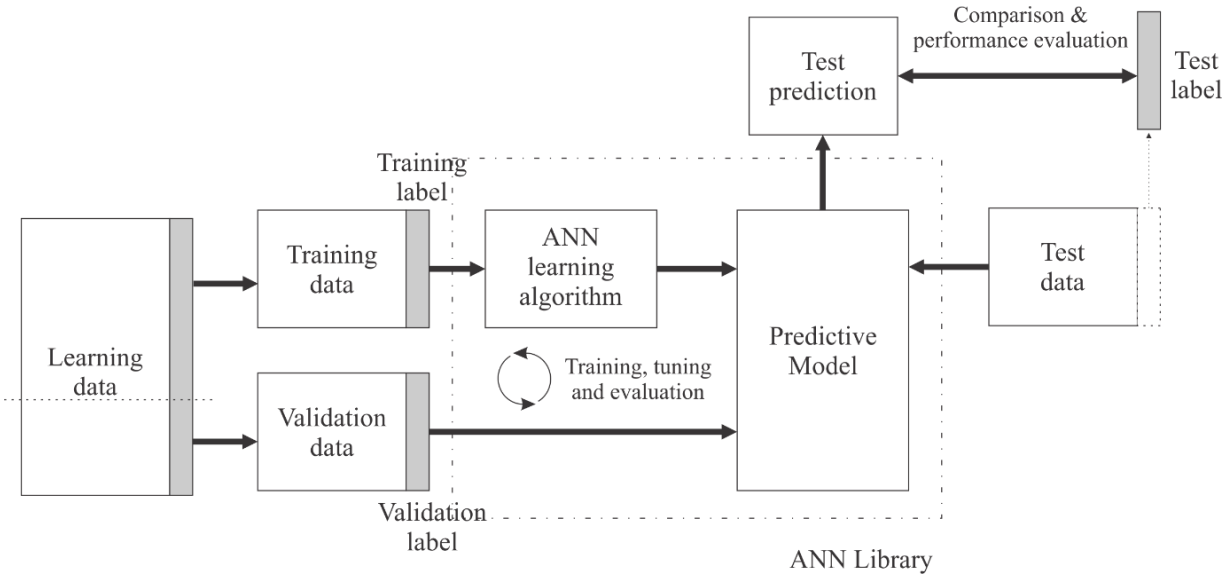

Figure 7. Flowchart of the general training, validation and test procedure.

In the output layer, the Softmax function S(y_i) is used for normalizing the values between 0 and 1, where the sum of the values is 1. Eq. (10) describes the function, where $y_{NN,i}$ is the value in the neural network (NN)'s output layer.

$$S(y_{NN,i}) = \frac{e^{y_{NN,i}}}{\sum_{j=1}^{n} e^{y_{NN,j}}} \text{ , } i = 1, 2, \ldots, n \tag{10}$$

The training uses the cross-entropy loss function $L_{CE}(S, y_d)$, which is defined in Eq. (11), where n is the number of fault types, S_i is the i-th value in the output of the Softmax function, and $y_{d,i}$ is the i-th desired value in the labeled data.

$$L_{CE}(S, y_d) = -\frac{1}{n}\sum_{i=1}^{n}\left(y_{d,i} \log S_i + (1 - y_{d,i}) \log(1 - S_i)\right) \tag{11}$$

Figure 8 describes the convergence of the loss. The black and gray lines represent the training and validation losses, respectively. During the training process, the algorithm compute the validation loss for 1,000 iterations and the ANN was kept if the validation loss was lower than the known minimum value.

Supervised learning with labeled training data is used for building an ANN model with an input vector and a desired output value, which is called the supervisory signal in this paper. To obtain learning data for training and validation samples for fault diagnosis, we performed 1080 dynamic simulation cases (180 for each fault case) using Simo-Riflex [36, 37] with different combinations of 6 fault types, 18 wind & wave conditions, and 10 fault occurrence times. The terminologies are defined to avoid any confusion throughout this section.

- **Fault type**: considered faults described in Table 4
- **Fault occurrence time**: pre-selected time instants
- **Load case**: wind and wave conditions described in Table 3
- **Simulation case**: time-domain analyses for each load case and a given fault type at a given occurrence time
- **Sample**: a collection of time series of different response parameters with a given duration from simulation cases. Each sample corresponds to one data point of inputs in the ANN model for fault diagnosis.

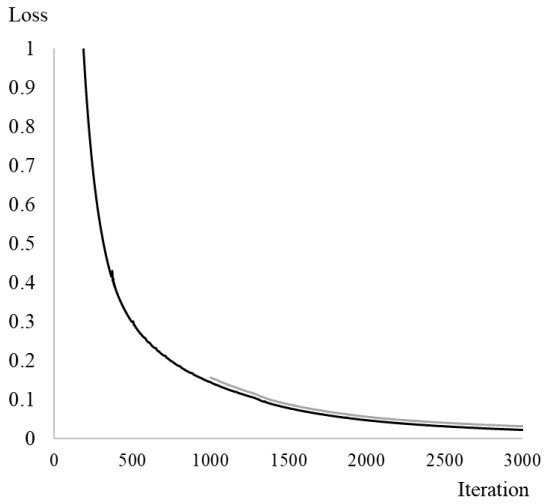

Figure 8. Convergence of the training and validation losses during the training of the ANN (black line: training loss, grey line: validation loss).

The runtime for each simulation case is 400 s which is long enough to obtain the correct response statistics and the simulation time interval is 0.1 s. The fault occurrence time is predetermined from 75 to 300 s with a 25 s interval for the training procedure. In each simulation case during the 400s, only one fault case is considered. For the test procedure, 144 new simulation cases are conducted and different independent wind and wave conditions are used compared to those of the simulations for training and validation.

The data sampling algorithm picks up multiple inputs for the ANN model in one simulation case. The starting point of the data sampling is randomly selected in the region of fault conditions after the fault occurrence time (TF) until the end of the simulation including the time interval of fault development. In the training procedure, every possible fault data should be trained by the algorithm after TF and for a sufficient time to escalate faults. Figure 9 shows the fault data sampling in a possible pick-up range. Once the algorithm picks up the starting point, the data can be observed during the sampling duration. For instance, from a starting point at 200 s after TF that is randomly selected, the sampling is conducted during the sampling duration. Additionally, the algorithm gathers the fault data to try not to totally duplicate the data which means that the starting point is not duplicated with each starting point. Based on this algorithm, training, validation, and test data were selected for machine learning and final performance evaluation. In Figure 9, the pattern of the sampling duration highlighted in blue is totally different from the pattern of multiple sampling in red in one simulation case. Figure 10 shows the extracted features from the sampling data based on the blade pitch sensor values, blade pitch commands, valve spool positions, and control input voltages.

A sample comprises a pair of datasets and labels. The dataset contains the pitch sensor, pitch command, valve position, and valve voltage values also used in each time interval $\Delta t_i = 0.1$. The dataset values are normalized between 0 and 1 using the minimum and maximum values of each observation element described in Eq. (12). The label indicates the fault type, which is represented by the one-hot encoding scheme [51]. This represents the i-th fault type using a vector of six binary values, in which only i-th value has 1 and the others have 0. Table 5 illustrates a learning data samples with 40000 samplings and 20 s sampling duration. In Table 5, for instance, the vector [1 0 0 0 0 0] in row 1 of the label indicates that the dataset is made when the wind turbine has fault type 1.

$$x_{i,normalized} = \frac{x_i - \min(x_i)}{\max(x_i) - \min(x_i)} \tag{12}$$

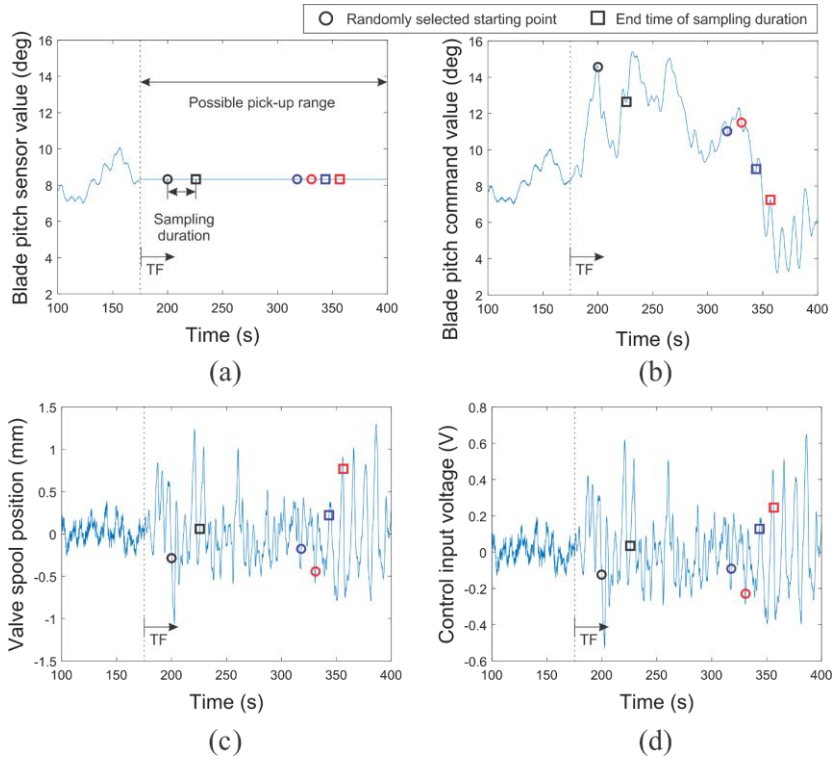

Figure 9. Fault data sampling in a possible pick-up range in the data from fault 2 (TF = 175 s): (a) blade pitch sensor value, (b) blade pitch command value, (c) valve spool position, and (d) control input voltage.

Table 5. Illustration of learning data samples with 40000 samplings and 20 s sampling duration.

# of Sample	Dataset				Label
	Time step 1	Time step 2	…	Time step 200	
1	$\beta_{1,1}$ $\beta_{C1,1}$ $x_{v1,1}$ $u_{v1,1}$	$\beta_{1,2}$ $\beta_{C1,2}$ $x_{v1,2}$ $u_{v1,2}$	…	$\beta_{1,200}$ $\beta_{C1,200}$ $x_{v1,200}$ $u_{v1,200}$	1 0 0 0 0 0
2	$\beta_{2,1}$ $\beta_{C2,1}$ $x_{v2,1}$ $u_{v2,1}$	$\beta_{2,2}$ $\beta_{C2,2}$ $x_{v2,2}$ $u_{v2,2}$	…	$\beta_{2,200}$ $\beta_{C2,200}$ $x_{v2,200}$ $u_{v2,200}$	0 0 1 0 0 0
⋮	⋮	⋮	⋱	⋮	⋮
n	$\beta_{n,1}$ $\beta_{Cn,1}$ $x_{vn,1}$ $u_{vn,1}$	$\beta_{n,2}$ $\beta_{Cn,2}$ $x_{vn,2}$ $u_{vn,2}$	…	$\beta_{n,200}$ $\beta_{Cn,200}$ $x_{vn,200}$ $u_{vn,200}$	0 0 0 0 1 0

To select the size of the dataset, the number of samples and duration of sampling should be determined. We train the ANN by increasing the number of samples from 40,000 to 100,000 of sampling size within theoretically 639,000 maximum sampling size in sampling duration from 10 to 20 s for 1080 simulation cases. The 20000 samples are used for validation. Table 6 describes the variables for the training, validation and test procedures from numerical simulations.

Table 6. The variables for training, validation and test.

	Training / Validation	Test
The number of simulation cases	1080	144
The number of samples	40,000 – 100,000 / 20,000	15,000
Distribution of input data	Uniform	Uniform
Min. criterion for model selection (%)	-	98

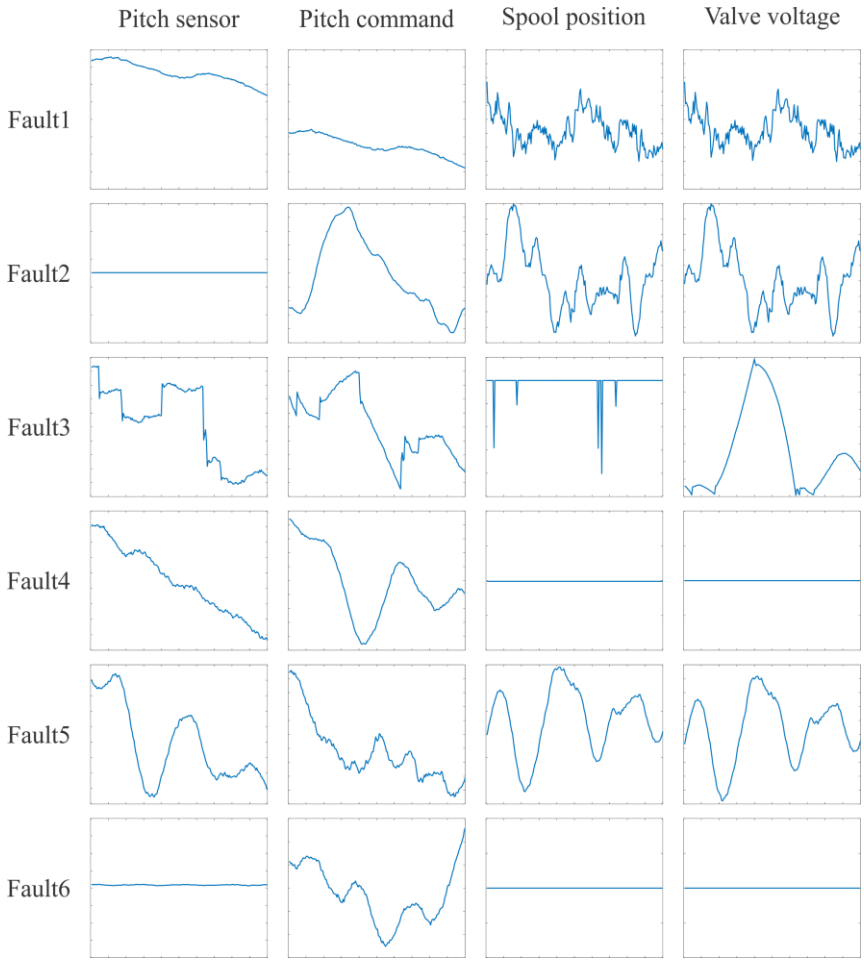

Figure 10. Extracted features from sampling data based on the physical values and faults.

Figure 11 shows the mesh surface and contour used to decide the number of samples and the duration of sampling in the validation procedure. This mesh surface is made by the data from an average value of the accuracy calculation in the training procedure which was conducted 10 times for each number of samples and sampling duration in Figure 9 (a). The target is above 98 % accuracy and two optimal points are selected as shown in Figure 9 (b).

From the results of Figure 11, five predictive models are selected based on the number of samples and sampling duration. To verify the performance of the models, the test procedure is essential to select the representative predictive model via 15000 test samples for the fault diagnosis scheme. The selected five predictive models have good performances in the test procedures above 98 % success rates and relatively small performance variations. The predictive model (P. Model) 2, which has a sampling duration of 20 s and a sample size of 90000 is chosen based on the best performance from the highest test success rate of 98.593 % among five predictive models.

Table 7. Test results.

	P. Model 1	P. Model 2	P. Model 3	P. Model 4	P. Model 5
No. samples	100000	90000	80000	90000	90000
Sampling duration (s)	20	20	20	19	17
Test success rate (%)	98.46 %	98.593 %	98. 153 %	98.433 %	98.24 %

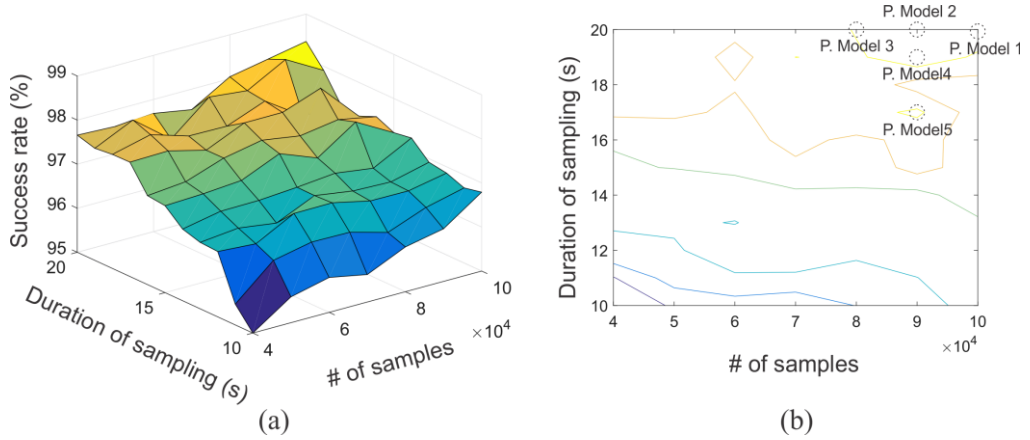

Figure 11. Success rate based on the number of samples and the duration of sampling in the validation procedure: (a) 3D surface and (b) contour.

3.4.2 Fault detection and diagnosis results

Basically, the fault diagnosis scheme was trained, validated, and tested with an ANN library based on TensorFlow [52] coded in Python. Then, the FDD scheme in Java code imports the optimized predictive model (predictive model 2) based on the test results from Table 7 exported from the ANN library. By optimizing the ANN model imported in Java code, fault diagnosis can be conducted in combination with Simo-Riflex with the same structure described in Figure 5 after successful fault detection. Figure 12 shows the data transmission between the ANN library and FDD scheme in Java for the optimized predictive model.

For fault detection and diagnosis, 60 simulation cases of each fault type simulated from the Simo-Riflex simulator were performed with a new wind profile generated by Turbsim and different fault occurrence times. Note that the fault diagnosis algorithm can be activated after the fault detection signal occurs. Figure 13 shows fault detection and diagnosis in real-time. In Figure 13 (a), Fault 1 (PSB) occurs after 150 s (time of fault, TF) corresponding to a -3° sensor bias on blade 3. Concurrently, the fault detection algorithm detects the fault at 153 s (time of fault detection, TFD), and the fault alarm is set to 1. Then the fault diagnosis algorithm is activated after the fault alarm occurs and diagnoses fault 1 at 170 s (time

of fault diagnosis, TFDI). Fault 3 (VEF) and Fault 5 (VWV) are detected and diagnosed with the same pattern in Figures 13 (b) and (c), respectively. After the time of fault diagnosis (TFDG), the operator can react and carry out shutdown or fault-tolerant control defending on the fault type. In pitch sensor faults (faults 1 and 2), fault-tolerant control using a virtual sensor [15] could be used to operate wind turbines without the faulty sensor [8]. Otherwise, the wind turbine should be shut down by a controller or operator under valve faults (faults 3 - 6) to avoid fault escalation.

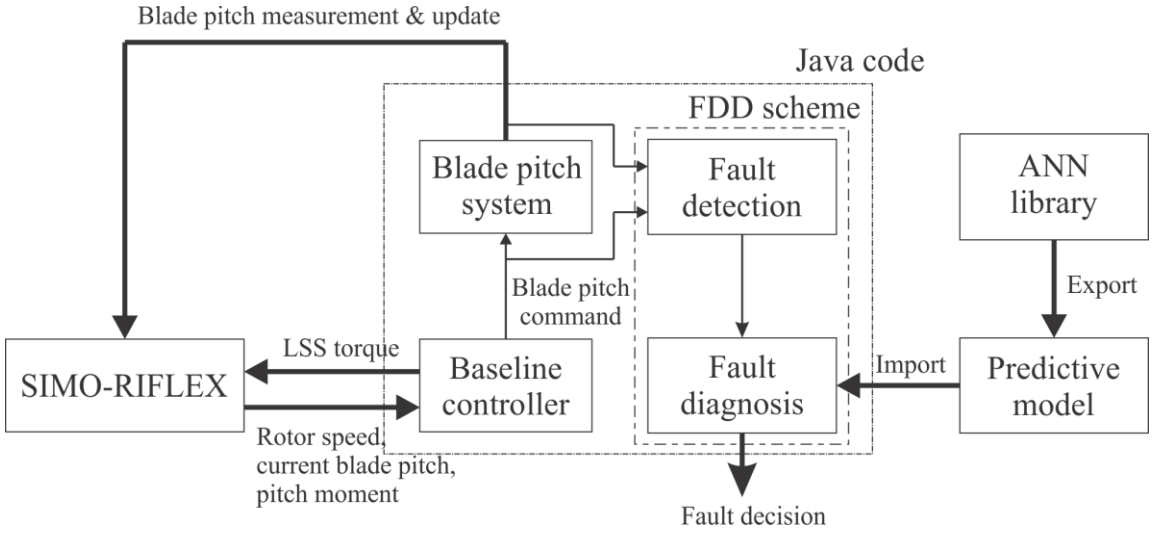

Figure 12. Data transmission among SR, Java code and the neural network model.

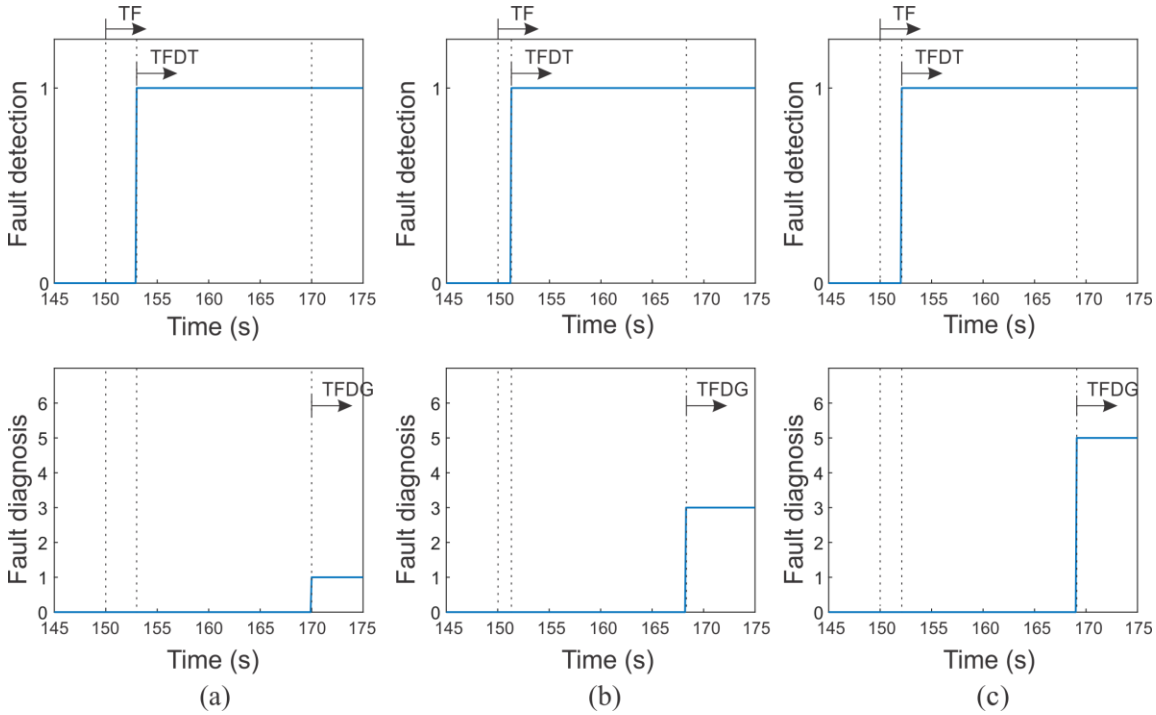

Figure 13. Fault detection and diagnosis in the faulty blade (blade 3) in real time: (a) fault 1 (PSB), (b) fault 3 (VEF), and (c) fault 5 (VWV).

Table 8 presents the fault diagnosis results obtained by the ANN scheme for a different set of examples corresponding to the blade pitch angle and valve spool position under different fault conditions. In this fault diagnosis procedure, one fault occur during one trial (simulation case). The fault occurrence time

is randomly selected in the above-rated region. In each fault type, the ANN is tested using 60 trials (10 trials for one load case described in Table 3) where the range of the rated wind speed (11.2 – 24 m/s) is correlated with wave conditions. The results indicate that the fault diagnosis model using the ANN scheme has a good performance of approximately 97.5% for the overall accuracy. Even though, the ANN scheme shows high accuracy, the scheme wrongly diagnoses faults at a rate of 2.5 % which is critical for the system.

Table 8. Fault diagnosis results.

	Fault 1	Fault 2	Fault 3	Fault 4	Fault 5	Fault 6
No. total trials	60	60	60	60	60	60
No. failures	2	1	0	3	1	2
No. successes	58	59	60	57	59	58
Rate (%)	96.667	98.333	100	95	98.333	96.667
Overall accuracy (%)			97.5			

Therefore, we built a system to correct the fault cases that were incorrectly diagnosed from the FDD scheme in more detail. In Figure 14, the number indicates the fault status, for instance, 0 for a fault-free state, 2 for fault 2 (PSF), and 6 for fault 6 (VCS). The red lines indicate the true status of the blade pitch system, and the blue lines indicate the diagnosis decisions made by the ANN. If the scheme makes a fault decision with little difference in the score in a vector in the ANN's output layer after the Softmax function procedure described in Eq. (10), the scheme automatically diagnoses twice more. Then the diagnosis scheme makes a final decision with the results of the three fault diagnosis tests. One interesting observation is that the ANN can make right decisions eventually, even if its initial decision is not correct. Another observation is that the pattern of the faults is similar. Based on these results, it should be noted that the proposed ANN-based fault diagnosis method presented here is capable of diagnosing faults properly in the operation of the monitored component. In addition, this approach was trained, validated and tested by numerical simulation for the simplest cases in the fault diagnosis. Once this algorithm builds an optimized model for fault diagnosis, this model can be applied to practical situations of wind turbine operation with real measurements from sensors.

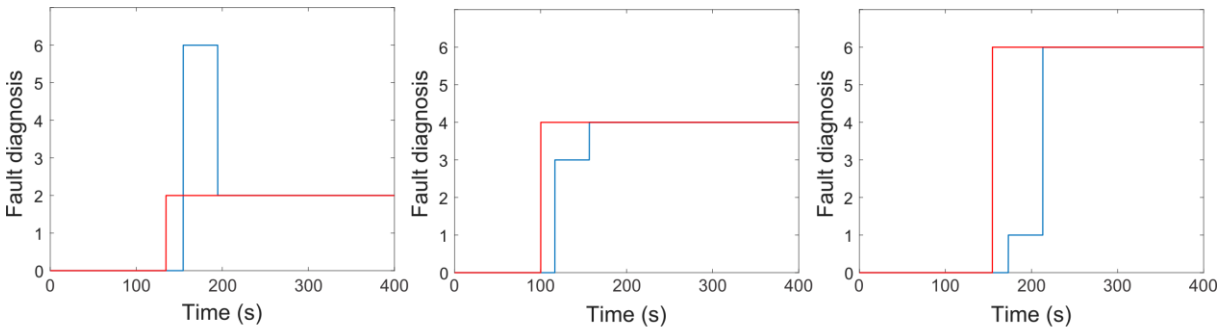

Figure 14. Fault diagnosis correction in the incorrect decision procedure (red line: true status, blue line: diagnosis decision): (a) fault 2 (PSF), (b) fault 4 (VSL), and (c) fault 6 (VCS).

4. Concluding remarks

This paper describes in detail a possible fault detection and diagnosis (FDD) approach for the blade pitch system in a spar-type floating wind turbine. The approach utilizes as a hybrid form based on a Kalman filter for fault detection and an artificial neural network for fault diagnosis. The Kalman filter estimates the blade pitch angle and valve spool position with measurements from appropriate sensors by considering the residuals and threshold. The pre-trained neural network models are used for fault diagnosis after successful fault detection. An artificial neural network learning algorithm use learning dataset from numerical simulation results to build the fault diagnosis scheme in the training, validation, and test procedures. The diagnostic performance of the optimized predictive model experimentally verified with the validation and test procedures shows 97.5 % of overall accuracy for each fault type.

This proposed method is built for fault diagnosis of simple fault cases. The purpose of this work is to build the ANN-based fault diagnosis scheme which can be extended to other applications. In future work, this FDD scheme will be modified to diagnose multiple fault cases among 6 fault types or other unknown faults in the blade pitch system in the wind turbine by simple changes of the model. Further studies will consider the application of the proposed solutions for practical models by data acquired from measurements on real installations. In addition, the method can offer a new general framework for a FDD application that can be applicable to other components, such as the drivetrain, generator, or yaw system in a wind turbine.

Acknowledgments

This work was supported by the MIT-NTNU-Statoil Wind Turbine Program (Project No. 40136503) funded by Equinor (formerly Statoil). The authors gratefully acknowledge the support of Equinor and the Research Council of Norway through the Centre for Ships and Offshore structures (CeSOS) and Centre for Autonomous Marine Operations and Systems (AMOS) at NTNU for the present study.

References

[1] Dinwoodie I, McMillan D, Revie M, Lazakis I, Dalgic Y. Development of a combined operational and strategic decision support model for offshore wind. Energy Procedia. 2013;35:157-66.

[2] Gayo JB. ‚Reliability-focused research on optimizing Wind Energy system design, operation and maintenance: Tools, proof of concepts, guidelines & methodologies for a new generation,“. Final Publishable Summary of Results of Project ReliaWind. 2011.

[3] Carroll J, McDonald A and McMillan D. Failure rate, repair time and unscheduled O&M cost analysis of offshore wind turbines. Wind Energy. 2016; 19; 1107-1119.

[4] NordzeeWind, Operations report 2009, Technical Report OWEZ_R_000_20101112, NordzeeWind, 2010.

[5] Cho S, Bachynski E, Rasekhi Nejad A, Gao Z, Moan T. Numerical modeling of hydraulic blade pitch actuator in a spar-type floating wind turbine considering fault conditions and their effects on global dynamic responses. Wind Energy 23 (2), 370-390.

[6] Isermann R. Fault-diagnosis systems: an introduction from fault detection to fault tolerance. Springer

Science & Business Media; 2006.

[7] Cho S, Gao Z and Moan T. Model-based fault detection of blade pitch system in floating wind turbines *Journal of Physics: Conference Series* 2016; **753** 092012.

[8] Cho S, Gao Z, Moan T. Model-based fault detection, fault isolation and fault-tolerant control of a blade pitch system in floating wind turbines. Renewable energy. 2018;120:306-21.

[9] Noshirvani, G, Askari, J, Fekih, A. A robust fault detection and isolation filter for the pitch system of a variable speed wind turbine. International Transactions on Electrical Energy Systems, 2018

[10] J. L. Godwin and P. Matthews, "Classification and Detection of Wind Turbine Pitch Faults Through SCADA Data Analysis," International Journal of Prognostics and Health Management, 2013.

[11] A. Kusiak and A. Verma, "A data-driven approach for monitoring blade pitch faults in wind turbines," IEEE Trans. Sustainable Energy, vol. 2, pp. 87-96, 2011

[12] Cong Yang, Zheng Qian, Yan Pei and Lu Wei, "A Data-Driven Approach for Condition Monitoring of Wind Turbine Pitch Systems," Energies, 2018

[13] Qiu Y, Chen L, Feng Y, Xu Y. An approach of quantifying gear fatigue life for wind turbine gearboxes using supervisory control and data acquisition data. Energies. 2017;10(8):1084.

[14] Chen W, Ding SX, Haghani A, Naik A, Khan AQ, Yin S. Observer-based FDI schemes for wind turbine benchmark. IFAC Proceedings Volumes. 2011;44(1):7073-8.

[15] Wei X, Verhaegen M, van Engelen T. Sensor fault detection and isolation for wind turbines based on subspace identification and Kalman filter techniques. International Journal of Adaptive Control and Signal Processing. 2010;24(8):687-707.

[16] Hamadache M, Lee D. Wind turbine main bearing fault detection via shaft speed signal analysis under constant load. In2016 16th International Conference on Control, Automation and Systems (ICCAS) 2016 Oct 16 (pp. 1579-1584). IEEE.

[17] Nejad AR, Odgaard PF, Gao Z, Moan T. A prognostic method for fault detection in wind turbine drivetrains. Engineering Failure Analysis. 2014;42:324-36.

[18] Wason R. Deep learning: Evolution and expansion. Cognitive Systems Research. 2018 Dec 1;52:701-8.

[19] Blanke M, Kinnaert M, Lunze J, Staroswiecki M, Schröder J. Diagnosis and fault-tolerant control. Berlin: springer 2006.

[20] Santos P, Villa L, Reñones A, Bustillo A, Maudes J. An SVM-based solution for fault detection in wind turbines. Sensors. 2015;15(3):5627-48.

[21] Zeng J, Lu D, Zhao Y, Zhang Z, Qiao W, Gong X. Wind turbine fault detection and isolation using support vector machine and a residual-based method. In2013 American Control Conference 2013 Jun 17 (pp. 3661-3666). IEEE.

[22] N. Laouti, N. Sheibat-Othman, and S. Othman, “Support vector machines for fault detection in wind turbines,” in Proc. IFAC World Congress, Sept. 2011, pp. 8295-8300.

[23] Badihi H, Zhang Y, Hong H. Wind turbine fault diagnosis and fault-tolerant torque load control against actuator faults. IEEE Transactions on Control Systems Technology. 2014 Dec 2;23(4):1351-72.

[24] Simani S, Farsoni S, Castaldi P. Fault diagnosis of a wind turbine benchmark via identified fuzzy models. IEEE Transactions on Industrial Electronics. 2014 Oct 22;62(6):3775-82.

[25] Kusiak A, Li W. The prediction and diagnosis of wind turbine faults. Renewable energy. 2011 Jan 1;36(1):16-23.

[26] Wang L, Zhang Z, Long H, Xu J, Liu R. Wind turbine gearbox failure identification with deep neural networks. IEEE Transactions on Industrial Informatics. 2016 Sep 8;13(3):1360-8.

[27] Zaher AS, McArthur SD, Infield DG, Patel Y. Online wind turbine fault detection through automated SCADA data analysis. Wind Energy: An International Journal for Progress and Applications in Wind Power Conversion Technology. 2009 Sep;12(6):574-93.

[28] Kusiak A, Verma A. Analyzing bearing faults in wind turbines: A data-mining approach. Renewable Energy. 2012 Dec 1;48:110-6.

[29] Bach-Andersen M, Winther O, Rømer-Odgaard B. Scalable systems for early faultdetection in wind turbines: a data driven approach. In: Proceedings of the annual conference of the European wind energy association; 2

[30] Bach-Andersen M, Rømer-Odgaard B, Winther O. Deep learning for automated drivetrain fault detection. Wind Energy. 2018 Jan;21(1):29-41.

[31] Tautz-Weinert J, Watson SJ. Comparison of different modelling approaches of drive train temperature for the purposes of wind turbine failure detection. InJournal of Physics: Conference Series 2016 Sep (Vol. 753, No. 7, p. 072014). IOP Publishing.

[32] Dervilis N, Choi M, Taylor SG, Barthorpe RJ, Park G, Farrar CR, Worden K. On damage diagnosis for a wind turbine blade using pattern recognition. Journal of sound and vibration. 2014 Mar 17;333(6):1833-50.

[33] Jiang G, Xie P, He H, Yan J. Wind turbine fault detection using a denoising autoencoder with temporal information. IEEE/Asme transactions on mechatronics. 2017 Oct 5;23(1):89-100.

[34] Jonkman J, Butterfield S, Musial W and Scott G. Definition of a 5-MW reference wind turbine for offshore system development *Technical Report NREL/TP-500-38060* USA, 2009

[35] Jonkman J. Definition of the floating system for Phase IV of OC3 *Technical Report NREL/TP-500-47535* USA, 2010

[36] SINTEF Ocean. SIMO 4.15.0 User Guide; 2018.

[37] SINTEF Ocean. RIFLEX 4.15.0 User Guide; 2018.

[38] Jiang Z, Karimirad, M and Moan T. Dynamic response analysis of wind turbines under blade pitch system fault, grid loss, and shutdown events. Wind Energy 2014; 17: 1385-1409. DOI: 10.1002/we.1639

[39] Cheng Z, Wang K, Gao Z, Moan T. A comparative study on dynamic responses of spar-type floating horizontal and vertical axis wind turbines. wind energy. 2017 Feb;20(2):305-23.

[40] Larsen TJ and Hanson TD. A method to avoid negative damped low-frequency tower vibration for a floating, pitch controlled wind turbine. Journal of Physics: Conference Series. 2007; **75** 012073.

[41] Jonkman J and Kilcher L. TurbSim User's Guide Technical Report NREL USA, 2012.

[42] IEC 61400-1: Wind turbines – part 1: Design requirements. International Electrotechnical Commission. 2005.

[43] IEC 61400-3: Wind turbines – Part 3: Design requirements for offshore wind turbines. International Electrotechnical Commission. 2005.

[44] Hasselmann K, Barnett TP, Bouws E, Carlson H, Cartwright DE, Enke K, Ewing JA, Gienapp H, Hasselmann DE, Kruseman P, Meerburg A. Measurements of wind-wave growth and swell decay during the Joint North Sea Wave Project (JONSWAP). Ergänzungsheft 8-12. 1973.

[45] Johannessen K, Meling T, Haver S. Joint distribution for wind and waves in the northern North Sea. International Journal of Offshore and Polar Engineering. 12(1).1-8.

[46] T. Esbensen, C. Sloth, Fault Diagnosis and Fault-tolerant Control of Wind Turbines, Master's thesis, Aalborg University, Aalborg, Denmark, 2009.

[47] Directional control valves, pilot-operated, with electrical position feedback and integrated electronics (OBS): RE29093, Rexroth, 2016.

[48] Karpenko M, Sepehri N. Fault-tolerant control of a servohydraulic positioning system with crossport leakage. IEEE Transactions on Control Systems Technology. 2005 Jan;13(1):155-61.

[49] Faragher R. Understanding the basis of the Kalman filter via a simple and intuitive derivation. IEEE Signal processing magazine. 2012;29(5):128-32.

[50] Krizhevsky A, Sutskever I, Hinton GE. Imagenet classification with deep convolutional neural networks. Advances in neural information processing systems. 2012, 1097-1105.

[51] Harris D, Harris S. Digital design and computer architecture. Morgan Kaufmann; 2010.

[52] Tensorflow tutorial. https://www.tensorflow.org/tutorials